

# Electric Field Imaging Pretouch for Robotic Graspers

Joshua R. Smith, Eric Garcia, Ryan Wistort, and Ganesh Krishnamoorthy

**Abstract**—This paper proposes the use of Electric Field Sensors to implement “pretouch” for robotic grasping. Weakly electric fish use this perceptual channel, but it has not received much attention in robotics. This paper describes a series of manipulators each of which incorporates Electric Field Sensors in a different fashion. In each case, the paper presents techniques for using the sensors, and experimental data collected. First, a simple dynamic-object avoidance technique is presented. Next, a 1-D alignment task for grasping is described. Then linear and rotary electrode scanning techniques are presented. It is shown that these techniques can distinguish a small object at close range from a large object farther away, a capability that may be important for grasping.

## I. INTRODUCTION

Vision is a long range sense with high spatial resolution. Tactile sensing can also provide high resolution spatial information, but at a range of zero. This paper explores the use of Electric Fields to provide a sense of “pretouch,” with range intermediate between vision and contact-based touch sensing. Using pretouch, a robotic grasper could align itself with a target object, and pre-shape appropriately to prepare for a successful grasp. The difficulty with relying on contact-based tactile sensing for these purposes is that touching the object may change its pose.

Weakly electric fish such as *Eigenmannia virescens* are able to sense their natural environment by generating electric fields and measuring perturbations in the field caused by nearby objects.[1] This perceptual channel has received little attention in robotics, perhaps in part because humans are unable to sense electric fields. Although animals are not known to use this sense for grasping, it appears to be well-suited to guiding grasping in incompletely known environments.

This paper describes initial experiments with electric field sensors integrated into a manipulator. The sophistication of the mechanical systems and of the data interpretation increases with each experiment. In the first set of

experiments, a single degree of freedom rotary robot arm avoids a human hand using simple thresholding operations on the sensor values. In the second set of experiments, a planar manipulator aligns itself with an object by estimating the target object’s position in one dimension from the sensor values. The third set of experiments uses a manipulator with electrodes built into the fingers, and a wrist that can rotate them. This experiment shows that either rotating the electrodes or changing the spacing between them can discriminate between the case of a small object close to the gripper, and a large object at longer range. We believe this capability will be important for pre-touch-based grasping.

## II. ELECTRIC FIELD SENSING AND IMAGING

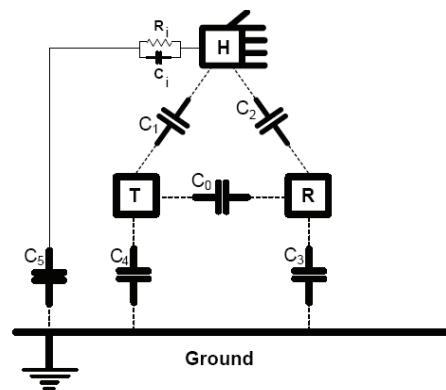


**Fig. 1:** Lumped circuit model for electric field sensing of a hand. When the hand (or other sensed object) moves closer to the sensor electrode pair (labeled T for Transmit and R for Receive), the received signal decreases because more displacement current is shunted to ground.

In Electric Field Sensing, illustrated in Figure 1, a low frequency (100KHz) AC voltage is applied to a transmit electrode (labeled T), which via capacitance  $C_0$  induces a displacement current in the receive electrode (labeled R).[2] The position of the hand (labeled H) relative to T and R modifies the capacitance  $C_0$  between T and R, and thus the amplitude of the signal received at R. If the hand is grounded (as shown in the figure), the displacement current received at R decreases as the hand approaches the electrodes.

Electric Field Sensing is well-suited to measuring conductive objects, as well as objects whose dielectric constant is substantially different than the surroundings. In practice, metals, the human body, fruits and vegetables, and water-based liquids all work well because of their high

Manuscript received September 15, 2006. This work was supported by Intel Research.

Joshua R. Smith is a senior researcher with Intel Research Seattle, WA 98105 USA (corresponding author Phone: 206-633-9900; fax: 206-633-6504; e-mail: [joshua.r.smith@intel.com](mailto:joshua.r.smith@intel.com)).

Eric Garcia is a doctoral student in the Department of Electrical Engineering (email: [eric.garcia@gmail.com](mailto:eric.garcia@gmail.com)).

Ryan Wistort is a student at the University of Washington in the Department of Electrical Engineering (email: [Ryan@RyBOTS.com](mailto:Ryan@RyBOTS.com)).

Ganesh Krishnamoorthy is a doctoral student in the Mechanical Engineering Department, University of Texas at Austin, Austin, TX 78712 USA (e-mail: [ganeshk@mail.utexas.edu](mailto:ganeshk@mail.utexas.edu)).

conductivity and/or dielectric contrast. Thin plastic cases, fabric, thin sheets of paper and thin glass cannot be sensed well (thin means relative to the electrode spacing). On the positive side, this means that Electric Field Sensing can operate through thin layers of plastic, fabric, paper, or glass if desired.

Because it fundamentally measures capacitance, Electric Field Sensing is a form of capacitive sensing. However, the term capacitive sensing most commonly refers to measuring the current out of electrode T. In such traditional capacitive sensing systems, N electrodes provide N measurements. In a pairwise Electric Field Sensing system, N transmitters and M receivers allow  $N \cdot M$  measurements.

*A note on terminology:* In this paper, the term Electric Field Sensing refers to this pairwise sensing mechanism; Electric Field Imaging is the higher level perceptual processes necessary to interpret the data. It has previously been demonstrated in [2] that with an array of field measurements, Electric Field Imaging can simultaneously track the position and orientation of two hands. Thus by processing multiple electric field measurements in a sophisticated fashion, Electric Field Imaging can infer much more complex geometrical information than a simple proximity measurement.

### III. RELATED WORK

Electric Field and capacitive sensing has been explored in robotics in a few different contexts: whole arm obstacle avoidance, safety, and seam-following. The references discussed here are meant to be representative rather than exhaustive. Novak and Feddema [3] describe an 8 channel Electric Field sensor system (that uses pairwise measurements) for obstacle avoidance in a whole-arm manipulator. Karlsson [4] describes a capacitive safety system that detects humans in the workspace of an industrial robot, shutting down the robot if a human enters the workspace. Schmitt et al. [5] describe a capacitance-based seam tracking system for dispensing brazing paste with high precision and high speed for rocket thrust chamber manufacturing. Mauer [6] described an end effector with an array of single-electrode capacitive sensors. The sensor information from the array was used only to form an “image,” and was not used for control purposes. More recently, Solberg, Lynch, and MacIver demonstrated robotic electrolocation for an underwater robot.[7]

Our first experiment can be viewed as a form of obstacle avoidance. In Novak and Feddema, a desired manipulator path is modified to avoid static obstacles. In the first experiment, there is no-preplanned trajectory. The “obstacles” are dynamically moving objects (human hands). The interaction of the manipulator with the dynamically moving human hands determines the manipulator’s dynamics. The second experiment has some features in common with the seam-tracking system of Schmitt et al [5]. Both use Electric Field measurements for tracking, rather

than avoidance. However [5] is clearly not a grasping task. As far as the authors know, the object alignment experiment reported here is the first use of capacitive sensing or Electric Field Sensing to guide grasping, rather than to avoid obstacles.

### IV. SENSING APPARATUS

The sensing for the experiments reported here was implemented with the LazyFish Electric Field Sensing board, pictured in Fig. 2. It has 4 resonant transmit channels (shown schematically in Fig. 3) that operate at 100KHz, and 2 receive channels consisting of transimpedance amplifiers followed by additional voltage gain (shown schematically in Fig. 4) and then analog to digital conversion in a microcontroller. This receive chain measures current induced on the receive electrode by the transmit electrode. The microcontroller processes the samples from the ADC to implement a phase sensitive undersampled form of synchronous detection. This detection technique rejects low-frequency “1/f” noise and 50Hz / 60Hz noise, yet requires very few external components because the demodulation operation is performed in software on the microcontroller. The resonant drive boosts the signal strength from 5V to approximately 100V, which is crucial to achieving high-sensitivity, long-range measurements. In the first two experiments, the electrodes were made of copper tape. In the third experiment, electrodes were formed from a section of copper tubing embedded in the plastic fingers. Microphone cable (which is shielded yet much more flexible than typical coaxial cable) was used to connect the electrodes to the LazyFish sensing board.

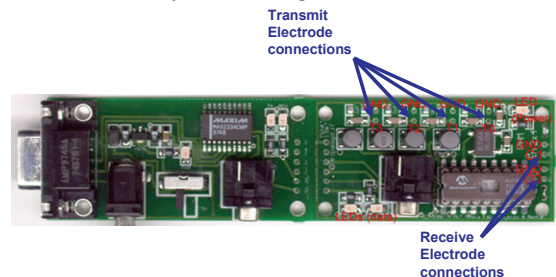


Fig. 2: Photograph of LazyFish Electric Field Sensing board

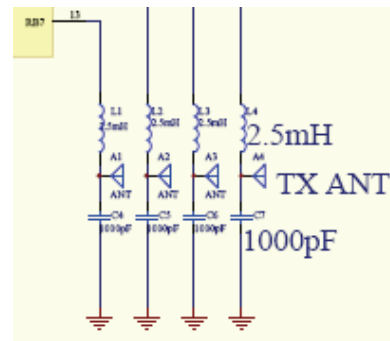


Fig. 3: Four transmit channels. Each is driven by a microcontroller output pin (not shown).

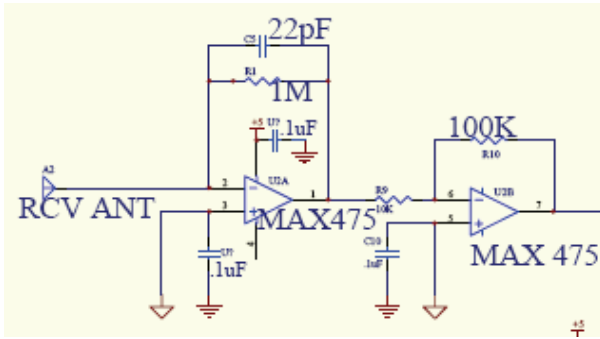


Fig. 4: One of two receive chains. The output of the second operational amplifier feeds into an ADC input on the microcontroller (not shown).

## V. SENSOR PHYSICS: FORWARD PROBLEM

In principle, the behavior of the sensors can be predicted by solving Laplace's equation  $\nabla^2 V \equiv \nabla \cdot \nabla V = 0$  for the boundary conditions determined by the sensor electrodes and the objects being sensed. (Technically Laplace's equation only applies to electrostatic systems. The system's measurement frequency is 100KHz, corresponding to a wavelength of 3Km, very long compared with the robot geometry. This is known as the electro-quasistatic regime. Induced currents in this regime are proportional to induced charges in the electrostatic case, so Laplace's equation can be used.) The sensor electronics maintains the receive electrodes at 0V. The drive circuitry puts the transmit electrode at some non-zero voltage. If the objects being sensed are sufficiently well-coupled to ground, then the sensed object is also at 0V. (The human body, and any conductive object held by a human, in typical room environments is coupled capacitively to ground well enough to be sensed in this fashion. The object being sensed may also be coupled to [robot] ground through parts of the robot, such as its palm. More detailed investigation of conditions under which objects are or are not sufficiently grounded will be addressed in future work.) The measured sensor value is proportional to the charge induced on the receive electrode. To find the induced charge, first solve Laplace's equation for the appropriate boundary conditions. This defines the potential  $V(x)$  (a scalar field) at every point in space. The electric field is the gradient of the potential:  $E = \nabla V$ , a vector field. Finally, integrate the electric flux through a Gaussian surface surrounding the receive electrode. By the divergence theorem, this gives the charge on the receive electrode.  $Q = \oint_S E \cdot ds$ , where  $S$  is a surface enclosing the

electrode. Because we are in the electro-quasistatic regime, we measure a current that is proportional to the charge  $Q$  that would be found in the purely electrostatic case.

Suppose that every configuration of the electrodes and the objects being sensed can be expressed by some parameterized geometrical model. The geometry defines boundary conditions for Laplace's equation. With the boundary conditions specified, Laplace's equation

determines the value of the field  $V$  at every point in space, beyond the boundaries, and thus by the calculations explained above, the sensor values are determined.

There are many known techniques for solving PDEs such as Laplace's equation. In this paper, we have used a new technique that will be reported in detail in future publications. Our hope is that this method will compare favorably in the ratio of performance to accuracy, but we have not yet validated this assertion. The basic idea is to find a set of charges (positions and strengths) such that the superposition of each of their individual fields

$$V(r) = \frac{q}{r}$$

produces a  $V=0$  iso-surface with the geometry of the original problem. In this sense the technique is like the method of images, but uses a different construction than the series of images of [2]; the new technique allows modeling of much more complex geometry than [2].

In our approach, the surface of the each grounded object is sampled by  $N$  points  $\{s_1, \dots, s_N\}$ . Thus, we find the set  $M$  of point charge locations  $\{x_1, \dots, x_M\}$  and strengths  $\{q_1, \dots, q_M\}$  that force the voltage at each  $s_i$  to the potential  $v_i$  of the object from which it was sampled.

While this problem is linear in the charge strengths  $q_j$ , it is non-linear in the charge positions  $x_j$ . By a further approximation, we fix the charge locations a priori by sampling  $M$  locations inside each object. Thus the optimal charge strengths  $\{q_1^*, \dots, q_M^*\}$  at the sampled charge locations  $\{x_1, \dots, x_M\}$  that match the sampled boundary conditions  $\{s_1, \dots, s_N\}$  are the solution to the following linear program:

$$\{q_j^*\} = \arg \min_{\{q_1, \dots, q_M\}} \sum_i^N \left| \sum_j^M \frac{q_j}{\|s_i - x_j\|_2} - v_i \right|$$

In this model, the current measured at the receiver  $R$  (or any object) is given by the sum of charge strengths inside the object:

$$i_R \propto Q_R = \sum_{\{j|x_j \in R\}} q_j.$$

## VI. INFERENCE: INVERSE PROBLEM

Given a set of measured sensor values, the parameter space can be searched to find the best explanation for the data. Although it is not clear how to give general conditions that guarantee a unique parameter-space inverse for every valid point in sensor space, for any proposed measurement scheme, it is possible to test numerically whether a unique inverse exists. If one does not, additional measurements can be added to break remaining degeneracies.

In practice, a single TX-RCV electrode pair has an iso-signal surface that is approximately ellipsoidal (for a sensed object that is small compared to the electrode spacing). The long axis of the ellipsoid is coincident with the line that passes through the TX and RCV electrodes. Assuming for the moment that one is interested only in object position (and not size or other parameters), then each sensor

measurement constrains the object to a location on an ellipsoidal shell. Larger sensor values correspond to larger shells nested around the pair of measurement electrodes. The set of feasible object locations is the intersection of the measurement shells. Examples of these ellipsoidal iso-signal surfaces may be found in [8], pps. 601-602. Another example is shown in Fig. 5 below.

Apart from the example figure below, this initial paper does not present any results on solving the inverse problem; that will be the subject of future work.

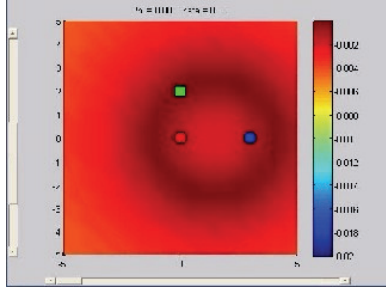


**Fig. 5:** Ellipsoidal iso-signal surface from a single measurement. The two circles (red and blue) on the center horizontal axis of the image are a transmit and a receive electrode. The third circle (green), above the electrode in the center of the image, is the true position of an object being sensed. The plot shows the squared error between the sensor value for the true position and the sensor value for each hypothesized position (i.e., the sensed value expected if the object had been at the plotted location). The dark ring thus represents the set of locations consistent with the observed value. The center of the ring is the iso-signal surface; the thickness of the ring represents the uncertainty in the position estimate. In this figure the noise has been exaggerated to make the image readable. Additional measurements shrink the seat of feasible object locations.

### VII. HUMAN HAND AVOIDANCE EXPERIMENT

A simple robot “arm” with one rotational degree of freedom was constructed. This apparatus is shown in the associated video. A transmit-receive pair of electrodes was placed on each side of the arm. Each electrode was 0.75” x 0.75”, with a center-to-center spacing of 2”. After recording a baseline value  $B_i$  for each channel  $i$  with no object nearby, the quantity  $B_i - v_i$  (where  $v_i$  is the raw sensor value) was used as the hand proximity estimator.

When both baseline-subtracted sensor values are below a threshold near zero (the “object present” threshold), it means that the hand is not present, so the robot remains stationary. The “object present” threshold is necessary to prevent the robot from moving randomly when no hand is present. If either sensor value is above the “object present” threshold, then the robot takes a fixed-size angular step in the direction that decreases the absolute value of the difference between the sensor values. When the difference is below a second threshold (the “centered” threshold), the robot arm will stop. Thus if a human hand is brought to the right side of the robot arm, and there is no hand on the left, the robot will take a series of steps to the left, until it is far enough from the hand to be below the “object present” threshold. If there are hands on both sides of the robot, but the hand on the right side is closer, the robot will move left. If the hands are

placed symmetrically on both sides of the arm, the difference in sensor values will be below the “centered” threshold and the arm will not move. The associated video shows the hand interaction, which is also illustrated in Fig. 6, below.



**Fig. 6:** Human hand avoidance experiment. As the human hand approaches the robot arm, the robot arm moves away.

### VIII. 1-D ALIGNMENT EXPERIMENT

Fig. 7 is a photograph of the apparatus for a 1-D alignment experiment. The experiment used a planar robot with 3 rotational joints, plus a simple parallel jaw gripper. The robot uses the joints to move linearly in one dimension, until it finds the closest point to the object along that line, at which time it can move in a second, perpendicular direction to get closer and attempt a grasp. The electrodes are visible in this image, but can be seen more clearly in the schematic Fig. 8.

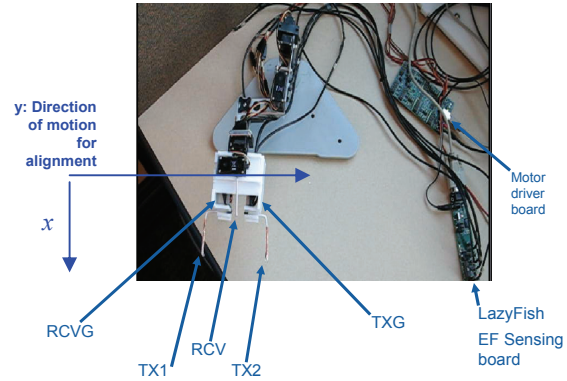


**Fig. 7:** Photo of planar manipulator with EF Sensing electrodes. TX1 and TX2 are (time multiplexed) transmit electrodes used for alignment. RCV is the receive electrode used for alignment. TXG and RCVG is an additional electrode pair intended to detect that the object is in range for grasping.

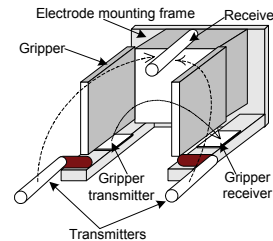


**Fig. 8:** Gripper diagram showing electrode geometry

A plastic enclosure around the parallel jaw gripper houses the electrodes. There are two sets of electrodes, one set for alignment with the object, and one to determine when to

execute a grasp. The alignment electrodes are stiff coaxial cable “whiskers” that extend forward 2” from the front of the end effector housing. The alignment electrodes are formed from copper tape that covers the front 1.75” of the outer surface of the coaxial cable. Each alignment electrode is connected to the center conductor of its coaxial cable. The second set of electrodes, used to determine when to close the gripper, are flat patches of copper tape 0.75” x 0.5”, located behind the alignment electrodes and below the gripper.

It turns out that for this particular sensor geometry, a very simple formula provides a good estimate of linear position near the electrodes. The estimator may be written as

$$s = \frac{R - L}{R + L} \quad (1)$$

where  $R$  represents the right sensor value and  $L$  is the left sensor value. It may be thought of as the imbalance between the values, normalized by the total response. One very nice feature of this estimator is that it is monotonically increasing, and thus in principle invertible. The estimator has a linear region between the peaks of the sensor response (where the inverse is robust and well conditioned), and flattens outside the sensor response peaks (so that the inverse becomes ill-conditioned). The quantity  $R-L$  alone (without the  $R+L$  denominator) is not monotonically increasing, so its inverse is not single-valued.

In fact, since this estimator will be used for proportional control, the fact that at large displacements the sign of the estimate is correct but the magnitude is wrong yields reasonable behavior. It simply means that there is a maximum step size that the actuator will take, after which a new and likely more informative sensor reading will be taken and used to plan the next motion.

One undesirable feature of the estimator is that it becomes undefined as the denominator approaches zero, which is what happens when there is no signal, i.e. when no object is present. For this reason it is necessary to compare the sum to a threshold, analogous to the “object present” threshold used in the first experiment, and suppress motion if the value is below the threshold. This prevents the gripper from moving randomly in response to noise.

The planar robot was commanded to move in a series of 0.75in steps from -4.5in to +3in, and to return to -4.5in after +3in. The -4.5in to +3in command range was chosen so that the actual realized motion, taking into account a kink at -1 and other actuation errors, would be approximately symmetrical about the sensors and explore most of both sensors’ field of view. (The kink was a non-ideal feature of this particular actuator. At around -1, a commanded small change in position caused the configuration of two joints to change in ways that produced no net linear motion.) At each position in the sequence, the arm stopped and the true position of the end effector (as opposed to the commanded position) was measured manually and recorded. While the

arm was stationary, 100 samples were collected from each sensor channel.

The standard deviation of each set of 100 sensor values is approximately 9 in amplitude units. The ratio of the maximum signal value to this noise figure gives the system’s peak Signal-to-Noise Ratio (SNR). The SNR is  $20 \log_{10}(1440/9)=44\text{dB}$  (using 20 because the input values are in amplitude units). (Technically this is actually the Contrast-to-Noise Ratio, since the signal values used have had a baseline subtracted. CNR is a more conservative and correct estimate of practically usable SNR in sensing systems that are based on attenuation, although it should be noted that this measure depends on the object being sensed, not just on the sensor alone.)

After a straightforward linear calibration step yielding scale and offset parameters, the calibrated estimator can be used to find object position in desired units given sensor values  $R$  and  $L$ .

Fig. 9 is a plot of the true, measured end-effector position for the 1200 sample sequence, along with the position computed from the sensor data using the calibrated estimator. There is generally good agreement between true and estimated values in the -2in to +2in range. As previously discussed, the estimates diverge from the correct values beyond the -2in to +2in window, because the object is essentially beyond the sensors’ “field of view.”

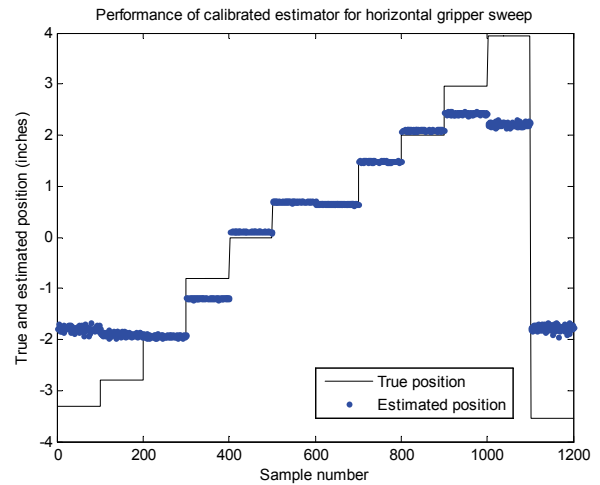


**Fig. 9:** Relative position (object with respect to grasper) estimated from sensors and true position for linear gripper sweep. An actuator kink produces the horizontal plateau in the center of the figure. As expected, the estimator response flattens outside the -2” to +2” range, resulting in the large errors at the extremes.

This simple estimator was used to implement a proportional controller for a grasping task. The end effector collects a sensor reading, uses the inverse estimator function to find the  $y$  coordinate of the object relative to the end effector, moves in the  $y$  dimension to the object’s estimated  $y$  position, and then collects another sensor reading. If the remaining estimator error is less than a threshold

(specifically if  $s < 0.1$ ) then the arm moves forward (in the  $x$  direction, as defined in Fig. 7) toward the object, and then repeats the  $y$  axis servoing procedure. At each step the forward  $x$  step does not occur until the  $y$  servoing procedure has reduced the estimator  $s$  error below 0.1. When the grasper sensor value exceeds a threshold value, the gripper is commanded to close. Fig. 10 shows the gripper closing around a broccoli stalk. The associated video shows the entire alignment and grasping process.

This servoing procedure strikes a good balance between speed and accuracy. It quickly and accurately aligns the end effector with the broccoli stalk. A previous attempt to perform the grasping task using a fixed horizontal step size (as in the first hand interaction experiment) was not successful. Because the actuator kinematics and dynamics are so uncertain, the only way to achieve the required fine motor control would have been to choose a fixed step size that was so small that the grasping procedure would not have seemed real time. The estimator and associated proportional control strategy presented here allowed the system to achieve real time grasping speed and accuracy despite very uncertain and unreliable actuators.



**Fig. 10:** Basic grasping after 1D alignment: the planar robot used the E-Field sensors to align itself with the target object before attempting the grasp.

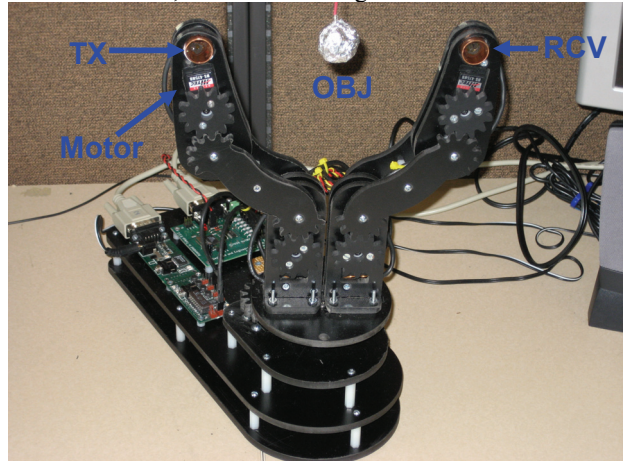
The grip closing sensor has room for improvement. Since it is mounted below the gripper, it is undesirably sensitive to small changes in the height ( $z$  position) of the object. Moving the gripper sensors to the back of the gripper paddles would be one way to improve this. A more robust differential measurement scheme similar to the one used for gripper alignment would be another way to improve the closure detection. The next set of experiments considers another more general solution to this problem.

## IX. LINEAR SCANNING EXPERIMENT

If the size of the object were known, then an absolute signal strength threshold could be used to determine when the target object was close enough to execute the grasp. But if the size is unknown, this simple technique will not work: a small object close to an electrode pair can yield the same measured value as a larger object that is further away. Thus an absolute threshold tuned for a small object would cause the gripper to close prematurely when a large object was presented. Although a single measurement clearly cannot discriminate between a small, nearby object and a larger, farther object, multiple measurements can.

This section presents a more sophisticated EF-sensing gripper, and presents two electrode scanning patterns that can discriminate between the (small, close) and (large, far) cases. Future work will extend this to explicitly estimating object size and position from a vector of measurements.

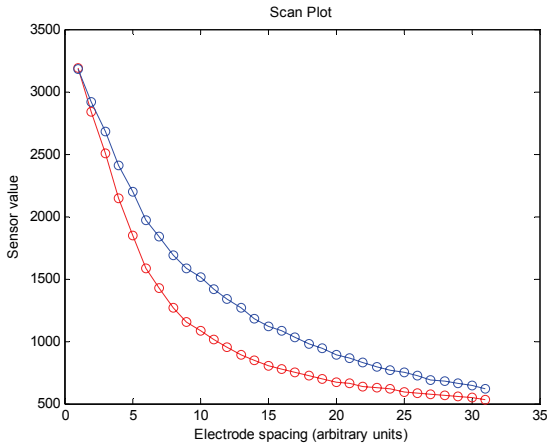
The EF sensing gripper shown in Fig. 11 has two fingers, each with two joints, and a wrist that can rotate the fingers through 180 degrees. The electrodes are sections of copper pipe embedded in the plastic fingers. This gripper is capable of changing the spacing between the electrodes, as well as rotating them.



**Fig. 11:** Photograph of EF sensing gripper including its base. A small test object (foil sphere) is shown between the fingers. The wrist below the gripper allows it to rotate the fingers 180 degrees, around the central axis. The data reported in the paper used spherical electrodes instead of the open cylinders shown in the image.

In the first experiment to demonstrate size-distance discrimination, the electrodes were initially placed close together (approximately 1 electrode diameter apart, 0.75in). A large object (3in diameter sphere) was placed above the electrode pair so that it was in range of the sensors. This initial sensor value was recorded. Then the electrode spacing was increased in 30 small increments until the inter-electrode spacing was approximately 5in. At each step the sensor value was recorded. Then the electrodes were returned to their initial 0.75in space, and a small object (1in diameter sphere) was placed above the electrodes, at a distance such that the sensor value was approximately the same as the initial sensor value had been for the large object. Thus by design this single initial measurement was unable to distinguish between the two cases. The electrode spacing was then changed in the same way. Fig. 12 shows the results of this experiment. It should be noted that the baseline coupling between the electrodes (that is, the sensor value even when no object is present) falls as the spacing is increased. In practice one would likely record the baseline (“no object present”) value for each separation and subtract measured values from that, but for clarity this has not been done in Fig. 12. Because of the large change in baseline value as the sensor spacing changes, it may not appear that there is much discrimination between these two cases, but in

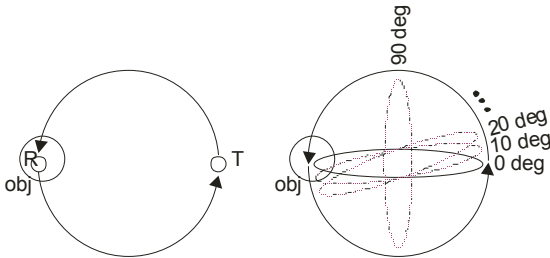
fact at around 10 on the horizontal axis (where the discrimination appears to be best), the sensor values differ by approximately 500, which is substantial: it is approximately 30% of the total sensor value of 1500 for the small ball (blue line) at 10, and about 50 times larger than the sensor noise.



**Fig. 12:** Using electrode spacing change to discriminate between a (small, close) object and a (large, far) object. The red line is the larger object.

### X. FIRST ROTARY SCANNING EXPERIMENT

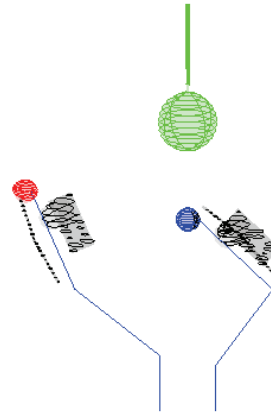
The gripper is also capable of rotating the electrodes. The aim of the next experiment is to determine whether it is possible to distinguish object size and distance by rotating the electrodes. In this experiment, the inter-electrode spacing was kept constant. This technique is potentially slightly simpler than the linear scan since it is not necessary to maintain a baseline. As shown in Fig. 13 and Fig. 14, the object was initially placed above the receive electrode, and the Transmit and Receive electrodes were rotated about the mid-point between them.



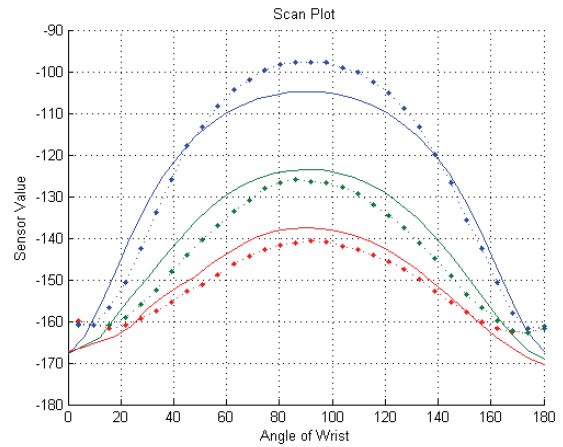
**Fig. 13:** A rotational scan for distinguishing object size and distance. The left figure shows the object position and electrode trajectory. The right figure shows an imaginary ellipsoidal iso-signal shell rotating with the electrodes. It is meant to illustrate how the sensitivity changes with electrode configuration. For a simplified model of sensor behavior, suppose that if the target object is outside the ellipse, it will not affect the sensors at all, and if it is inside the ellipse, it will affect the sensors.

Fig. 15 compares measured data and theoretical model for this experiment; the numerical model uses the new, fast image method for finding approximate solutions of Laplace's equation for complex geometries. Fig 14 shows

that the interior structure of the motors has been modeled; without detailed modeling, good agreement between model and data is not achieved. Clearly this measurement technique is capable of distinguishing these two cases. Although the discrimination looks substantial in the plot, it should be noted that the plot has much less dynamic range than Fig. 10, and the maximum difference in sensor values is only 100, or only about 5%.



**Fig. 14:** Electric field model of scanning geometry of Fig. 13. The receive electrode is the blue sphere. The transmit electrode (red sphere) rotates around the axis of the receive electrode and the target object. The cable suspending the sphere and the internal structure of the servo motors has been explicitly modeled.



**Fig. 15:** Discriminating object size and distance with a rotary scan. Spheres of radius 1cm [top, blue], 2cm [middle, green], and 3cm [bottom, red] were placed at distances of 3.5cm, 6.2cm, and 8.5 cm respectively above the sense electrodes. Measured sensor data (points) for rotational scan of Fig. 13 are plotted against theoretical model (solid lines) of same. The object heights were chosen so that at 0 degrees, the sensor values for the different sized objects would coincide.

### XI. SECOND ROTARY SCANNING EXPERIMENT

The next experiment explores another way to use electrode rotation. The geometry is shown in Fig. 16. In this case, the small (2 cm) object is placed at 90 degrees with respect to the transmitter, which will be rotated from 0

to 180 degrees about the receiver, which rotates in place at the origin. The object was placed at several different distances from the rotation axis. It may be surprising at first that the rotary motion of the first rotary scan experiment causes the sensor values to increase and then decrease (producing a “peak” shape), while the rotary motion of the second rotary scan experiment cause the sensor values to decrease and then increase (a “valley”). Comparing the trajectories of the iso-signal surfaces of Fig. 13 and Fig. 16 makes it apparent why this is the case: in the first example (Fig. 13), the object starts and ends inside the iso-signal ellipsoid, and is furthest from the ellipsoid when the sensors are at 90 degrees. In the second case (Fig. 16), the iso-signal ellipsoid overlaps with the object maximally at 90 degrees, and minimally at 0 and 180.

Fig. 17 shows the data from the second rotation experiment. The solid lines are the theoretical model, computed in the same way as the theoretical model of Fig. 15. The theoretical model has excellent qualitative and quantitative agreement with the data.

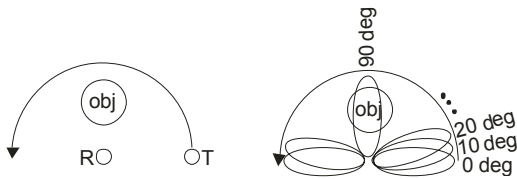


**Fig. 16:** A second rotational scan technique. The transmit electrode is rotated around the receive electrode. As in Fig. 11, illustrative iso-signal shells have been included.

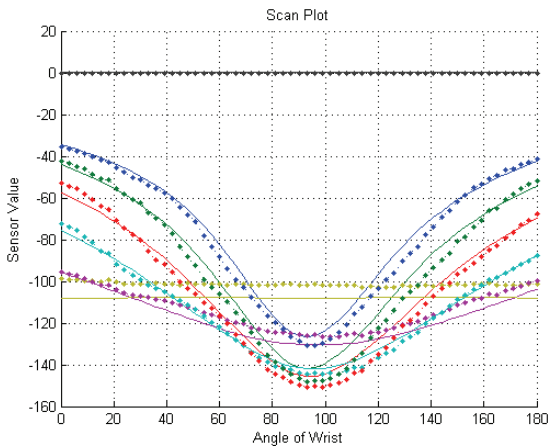


**Fig. 17:** Experimental data (points) and theoretical model (solid line) for the rotational scan of Fig. 16. A small (2 cm) object was placed at a height of 6.7 cm above and at 90 degrees to the TX, RCV pair. In each trial the object was placed at a different radial distance from the center of rotation (which coincides with the receive electrode). The colors blue, green, red, cyan, magenta, yellow, and black correspond to radial distances of 12.5 cm, 10.0 cm, 7.5 cm, 5.0 cm, 2.5 cm, 0.0 cm, and infinity.

## XII. CONCLUSION AND FUTURE WORK

This paper has presented a series of increasingly complex manipulators incorporating electric field sensors. First, a

simple dynamic-object avoidance technique was presented. Next, more complex planar manipulator used EF sensors for a 1-D alignment task. Next, an EF gripper with 2 fingers and a rotary wrist was presented. Linear and rotational scan experiments with this gripper show that both types of scan are capable of distinguishing a small object at close range from a large object at long range. Then experimental data and a theoretical model were presented for another type of rotary scan, with the object placed at several different radial distances.

The next step will be to use the model to quantitatively estimate geometrical object properties such as size and 3d position. Given the quantitative agreement between the data and forward model, it should be possible to provide good estimates of size and position. Note that the width of the “valleys” in Fig. 17 do not indicate the resolution of the sensing technique; rather, resolution is determined by our ability to discriminate among measurement vectors such as those plotted in Fig. 17. In future work on the inverse problem, we will investigate the precision and accuracy of position and size estimates. Also in future work, a Barrett Hand has been procured, to which Electric Field sensors will be added. The goal is to use such a system to implement E-Field guided grasps. One interesting future research problem is planning jointly for both information gain and grasping / manipulation. If pre-touch is deemed to be useful for grasping, we will also investigate complementary physical mechanisms so that it can be used with more materials,

The experiments presented in this paper have convinced the authors that Electric Field Imaging has promise for improving robotic grasping in unstructured environments.

## ACKNOWLEDGMENTS

We thank Ali Rahimi, Siddhartha Srinivasa, Bart Nabbe, and Dave Ferguson for helpful conversations and feedback.

## REFERENCES

- [1] Heiligenberg W (1973) Electrolocation of objects in the electric fish *Eigenmannia* (Rhamphichthyidae, Gymnotoidei). *J Comp Physiol* 87: 137-164.
- [2] Smith, J.R., “Electric Field Imaging,” Ph.D. Dissertation, Massachusetts Institute of Technology
- [3] Novak J., L., Feddema, I., T., “A capacitance-based proximity sensor for whole arm obstacle avoidance,” Proceedings of the 1992 IEEE International Conference on Robotics and Automation, pp 1307-1314, Nice, France, 1992.
- [4] N. Karlsson, “Theory and Application of a Capacitive Sensor for Safeguarding in Industry,” Proceedings of IEEE Instr. and Msmt. Technology Conf.--IMTC 94, Hammamatsu, Japan, May, 1994
- [5] D.J. Schmitt, J.L. Novak, G.P. Starr and J.E. Maslakowski, Real-Time Seam Tracking for Rocket Thrust Chamber Manufacturing, 1994 IEEE Robotics and Automation Proceedings.
- [6] G.F. Mauer, “An End-Effector Based Imaging Proximity Sensor,” *Journal of Robotic Systems*, 1989, pp301-316, Wiley & Sons.
- [7] J.R. Solberg, K.M. Lynch, M.A. MacIver, “Robotic Electrolocation: Active Underwater Target Localization with Electric Fields,” Proceedings of the 2007 International Conference on Robotics and Automation (ICRA) April 10-14, 2007, Rome Italy.
- [8] Smith, J.R., “Field Mice: Extracting hand geometry from Electric Field Measurements,” *IBM Systems Journal* Vol 35, Nos. 3&4, pp. 587-608. 1996.